Energy Conversion and Management 108 (2016) 336–347

Contents lists available at ScienceDirect

Energy Conversion and Management

journal homepage: www.elsevier.com/locate/enconman

An investigation on spray cooling using saline water with experimental verification

M.H. Sadafi [a,*], S. González Ruiz [b], M.R. Vetrano [b], I. Jahn [a], J. van Beeck [b], J.M. Buchlin [b], K. Hooman [a]

[a] School of Mechanical and Mining Engineering, The University of Queensland, QLD 4072, Australia
[b] von Karman Institute for Fluid Dynamics, Chausséede Waterloo 72, Rhode Saint Genèse, 1640, Belgium

ARTICLE INFO

Article history:
Received 31 August 2015
Accepted 10 November 2015
Available online 23 November 2015

Keywords:
Saline water
Spray cooling
Phase Doppler Interferometry
Discrete phase model
Heat and mass transfer

ABSTRACT

A natural draft dry cooling tower rejects heat in a power plant. Spray cooling of the inlet air to the cooling tower improves the total efficiency of the power plant. To overcome the scarcity of natural water sources, this research is studying the usage of saline water in spray assisted dry cooling towers. A nozzle is analysed experimentally. It is shown that the CFD model captures the spray well. A full cone spray is simulated in a vertical cylindrical domain representative of cooling tower flows. To investigate the influences of initial and ambient conditions on the spray performance, fourteen different cases are simulated and trends analysed. It is shown that the distances from the nozzle, after which the dry stream starts (wet lengths), are in the range of 4.3–5.25 m depending on the test conditions. A dimensionless study is performed on the wet length and cooling efficiency as the two main parameters. Finally, to predict the wet length and cooling efficiency, two dimensionless correlations are presented and their impact on cooling tower operation is discussed.

1. Introduction

Utilising saline water for spray cooling is an area that has received little attention, despite offering benefits both with respect to fresh water conservation and improvements in power generation efficiency. The aim of the current study is to improve the knowledge base associated with the use of saline water in spray cooling applications. An experimental study is performed to partially verify the presented CFD simulation of a single spray. After the reliability of the model was assured, the influence of initial and ambient condition on the spray performance was investigated and a practical analysis on the spray performance was made.

The outcome of this research is applicable in concentrated solar thermal (CST) power plants. In CST plants the hot temperature of the cycle reaches up to 600–700 °C [1]. Since the efficiency in a power plant is limited by Carnot efficiency ($1 - T_c/T_h$), to increase the total efficiency the cold temperature of the cycle should be decreased. To reduce the cold temperature (inlet air to the cooling tower), saline water spraying of the inlet air is suggested (Fig. 1) and studied in this work as a part of Australian Solar Thermal Research Initiative (ASTRI), a project supported by the Australian Government.

A CST plant is usually built in arid areas. Thus, a comprehensive study on evaporative spray cooling considers the scarcity of fresh water. To preserve the drinking water resources, and achieve an efficient performance, saline water is suggested for cooling purposes. In addition to performance improvement (8% higher cooling efficiency and 0.96 °C lower mean temperature [2]), using saline water instead of fresh water results in budget saving due to saving in natural water cost and generating excess electricity. In an economic study Ashwood and Bharathan showed that a 7.5 °C reduction in temperature due to spray cooling leads to 14% improvement in power generation rate in a 20 MW power plant [3]. Another study showed that, using sea water for cooling reduces the utility costs by 49.69% [4].

A drawback of using saline water is that heat exchanger surfaces are exposed to deposition and corrosion and solid particles (salt). To overcome these issues, in some cases such as in Condamine power station in Australia, corrosion is avoided using resistive materials (titanium condenser and fibreglass pipeline). Surface treatments [5–7] and controlling cooling water temperature [6,8] are the other methods. However, this work focuses on a design point of view to prevent the contact of wet droplets with the surfaces. This is done by ensuring that full evaporation is achieved before the sprayed stream reaches the metal surfaces. Here, the reactiveness of the saline solution is small [9].

* Corresponding author. Tel.: +61 7 3365 1661.
E-mail addresses: m.sadafi@uq.edu.au, mhsadafi@gmail.com (M.H. Sadafi), sara.gonzalez.ruiz@vki.ac.be (S. González Ruiz), vetrano@vki.ac.be (M.R. Vetrano), i.jahn@uq.edu.au (I. Jahn), vanbeeck@vki.ac.be (J. van Beeck), buchlin@vki.ac.be (J.M. Buchlin), k.hooman@uq.edu.au (K. Hooman).

http://dx.doi.org/10.1016/j.enconman.2015.11.025
0196-8904/

Nomenclature

A	surface area (m^2)
a_1, a_2, a_3	constants in drag coefficient calculation
c	mass concentration
c_p	specific heat (J/kg K)
C_1, C_2	non-dimensional constants
C_D	drag coefficient
$\bar{d}$	size constant (m)
D	diameter (m)
D_{32}	Sauter Mean Diameter, SMD (m)
f	frequency (Hz)
f_1, f_2	non-dimensional variables
F, G	non-dimensional functions
F_D	drag force per unit mass (m/s^2)
F_s	safety factor
GCI	grid convergence index
h	sensible enthalpy (J/kg)
h_{fg}	specific enthalpy of evaporation (J/kg)
$H_{lat,ref}$	latent heat at the reference conditions (J/kg)
H_{pyr}	heat of pyrolysis per unit mass (J/kg)
k	thermal conductivity (W/m K)
$\vec{l}$	unit vector of direction
L	distance (m)
L_{wet}	wet length (m)
m	mass (kg)
$\dot{m}$	mass flow rate (kg/s)
n	size distribution parameter
N	number of droplet
Nu	Nusselt number
p	order of convergence
Pr	Prandtl number
r	grid refinement ratio
Re	Reynolds number = $\frac{D_d u_r}{v_g}$
RH	relative humidity
Q	heat transfer (J)
t	time (s)
T	temperature (K)
u	velocity (m/s)
Y	mass fraction of droplets in the spray
ε	relative error of solution
$\eta_{Cooling}$	cooling efficiency (%)
θ	scattering angle
λ	wavelength (m)
μ	dynamic viscosity (kg/m s)
v	kinematic viscosity (m^2/s)
ρ	density (kg/m^3)
Ψ, Ω	non-dimensional numbers

Subscripts

0	initial condition
c	cold
D	Doppler shift
d	droplet
g	gas
h	hot
i	integer component
in	condition at entry of computational cell
l	illuminating beam
out	condition at exit of computational cell
r	relative
ref	reference
s	light scattered wavefront
w	water
wb	wet bulb

To correctly capture the physics of saline droplet evaporation, the evaporation process should be split into four stages: temperature adjustment, isothermal evaporation, transition to crust formation, and drying out [10]. A detailed study of single droplet evaporation by Sadafi et al. showed that for 500 μm radius saline water droplets, absorbed energy for evaporation decreases by up to 12.2% compared to pure water [11]. Moreover, due to crust formation, a dry stream achieves in an earlier time for saline water.

For the simulation of saline droplet evaporation in CFD, Sadafi et al. [2] developed and verified an approach that modifies the multicomponent discrete phase model (DPM) in ANSYS FLUENT [12]. After comparing the results obtained for 3% NaCl concentration (by mass) with pure water, they showed that using saline water shortens the length from the nozzle, covered by the wet stream. This allows designers to reduce the distance between the nozzle and the heat exchangers, thereby shortening cooling towers without loss of spray cooling efficiency.

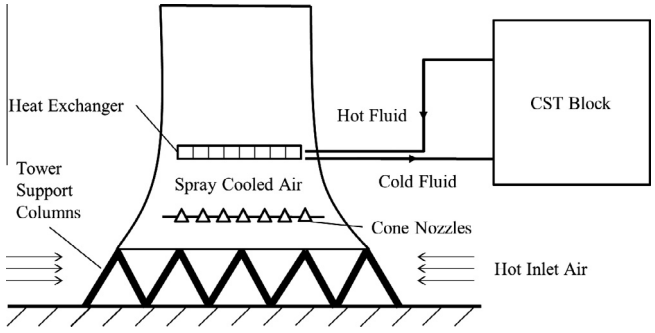

Fig. 1. Schematic cross-section of typical spray-assisted natural draft dry cooling tower.

To perform experimental studies on water spray systems, Phase Doppler Interferometry (PDI) is widely used by researchers. For example, Vetrano et al. used PDI to measure the size and velocity of the droplets in a full cone spray [13]. Using the Weber and Ohnesorge numbers, they presented a correlation to predict the Satur Mean Diameter (SMD) for a viscous liquid. Foissac et al. performed an experimental study on a single nozzle at high mass flow rate of 1 kg/s [14]. To obtain a local high resolution information about the spray, they used PDI and measured the size and velocity of the droplets passing through an optically defined probe volume. They reported no droplet at the core of the spray due to the hollow cone type of the nozzle. Therefore, the measurement were made in a ring and a Log-Normal distribution was observed for the droplet size distribution. Using PDI, Xie et al. investigated the thermal effects of a pressure swirl nozzle in spray cooling [15]. They reported that higher local droplet velocity occurs where there is a higher local droplet flux in the spatial distributions. Pawar et al. used PDI to validate their Euler-Lagrange model for a hollow cone pressure swirl nozzle spray [16]. They showed that, to obtain a reliable size and velocity for droplets, 5000 samples is adequate for each measurement.

In this study, the influences of initial and ambient conditions on the cooling performance of a single nozzle spray of NaCl–water solution are investigated. Firstly, using the experimental PDI results obtained in this study, a CFD model is partially validated. Then, after adjusting the geometry in the model, a wide range of initial conditions (for spray and ambient air) are simulated and non-dimensional analysis is applied to the data.

In this article, first, the numerical CFD model is explained. Next, the theory of the PDI method is given followed by the experimental study. Then, the results obtained from the experimental study are compared with those of CFD model. After verification of the CFD model, the sensitivity analysis of the numerical data is presented, and a discussion on the results is given.

2. Theory

2.1. Numerical model

To simulate the usage of saline water in spray cooling in a natural draft dry cooling tower, ANSYS FLUENT release 16.1 is used. The Eulerian–Lagrangian approach suggested by Nijdam et al. [17] is used and, the time-averaged Navier–Stokes equations with the standard k–ε model solves the turbulence model. The governing equations of the air flow and trajectory of a discrete phase droplets are presented in [2].

In the Lagrangian framework, the drag per unit droplet mass is given by [18]:

$$F_D = \frac{18\mu}{\rho_d D_d^2}\frac{C_D Re}{24}, \tag{1}$$

where drag coefficient, C_D is calculated as:

$$C_D = a_1 + \frac{a_2}{Re} + \frac{a_3}{Re^2}, \quad 0.1 \leqslant Re \leqslant 50,000. \tag{2}$$

Here a_1, a_2, and a_3 are constants, which correspond to spherical droplets. More information on determining these constants are available in [19].

Here, the gas and the droplets are the continuous and discrete phases, respectively. The heat transfer between these two phases is [18]:

$$Q = (m_{d,in} - m_{d,out})\left[-H_{lat,ref} + H_{pyr}\right] - m_{d,out}\int_{T_{ref}}^{T_{d,out}} c_p dT + m_{d,in}\int_{T_{ref}}^{T_{d,in}} c_p dT. \tag{3}$$

Here $H_{lat,ref}$ is the latent heat at the reference conditions for droplets. It is determined through the difference between liquid and gas standard formation enthalpies. Although it was shown that laser illumination dramatically increases the heat transfer rate in a single stationary droplet [20], it can be neglected in moving droplet, as the time under laser illumination is short [21].

Using the mass and momentum transfer equation presented in [2] the coupled heat transfer equation is:

$$m_d c_p \frac{dT_d}{dt} = hA_d(T_g - T_d) + \frac{dm_d}{dt}h_{fg}, \tag{4}$$

where $\frac{dm_p}{dt}$ is zero before the droplets heat up to reach the wet-bulb temperature.

To solve the couplings between velocity and pressure, the SIMPLE algorithm was used with a staggered grid. Turbulent kinetic energy and dissipation rate are solved using a first order upwind scheme, and second order upwind discretization is chosen for energy and momentum.

The Multicomponent Discrete Phase model in FLUENT requires each component to be a fluid. To consider the effect of NaCl in the process, a set of modifications are required. After performing a micro analysis using electron microscopy, Sadafi et al. [2] incorporated the solid (non-vaporizing) component in the droplet, as a liquid with the same density, thermal conductivity, and specific heat as NaCl. However, the vaporization temperature has been set to a proportionally infinity value to prevent the evaporation and phase change in the second component. Moreover, to correctly simulate the porosity of the dried crystal, the mass fraction of air in the solid part of the droplet was determined. Based on experimental data, a water droplet with 3% initial mass concentration of NaCl is composed of: 96.99% water, 3% NaCl, and about 0.01% trapped gas (mass fraction) [2]. This model was previously validated using the experimental results and numerical data obtained from a developed MATLAB model for a single droplet [11].

2.2. Phase Doppler Interferometry (PDI)

The Phase Doppler Interferometry is a laser based non-intrusive measurement technique that simultaneously measures the size and the velocity components of a moving droplet. This technique has been developed in the early eighties and today represents one of the most robust techniques to measure droplet size in two phase flows. The PDI technique is based on the phenomenon of elastic light scattering and, as all the techniques based on this physical phenomenon, suffers of some limitations. The main limitations are related to the maximum concentration of droplets in the probe volume and on their sphericity [22].

The technique is based on the frequency shift appearing in the scattered light wavefront respect to the incident wavefront. If a particle with $\vec{u}$ velocity is illuminated by a laser beam with the frequency of f_0 and wavelength of λ_0, the light is scattered in all directions. Considering $\vec{l_i}$ as the unit vector corresponding to the direction of propagation of the illuminating beam and $\vec{l_s}$ as an arbitrary direction of the light scattered wavefront, the net change in frequency or Doppler shift is written as [22]:

$$f_D = f_s - f_0 = \frac{\vec{u}}{\lambda_0}(\vec{l_s} - \vec{l_i}) \tag{5}$$

Therefore the droplet velocity can be directly retrieved using the above equation provided that the illuminating and scattering directions are well known. In order to eliminate the dependence on the scattering direction, one could consider a system in which two illuminating beams are used (dual beam mode). Assuming that these beams come from the same source, i.e. they are coherent, and that they illuminate the droplet along two different directions $\overrightarrow{l_{i1}}$ and $\overrightarrow{l_{i2}}$, one can compute the field (λ_{s1}, f_{s1}) and (λ_{s2}, f_{s2}), scattered in the $\vec{l_s}$ direction as:

$$f_{sk} = f_0 + \frac{\vec{u}}{\lambda_0}(\vec{l_s} - \overrightarrow{l_{ik}}) \quad \forall k \in \{1,2\} \tag{6}$$

And the shift in frequency f_D is [22]:

$$f_D = f_{s2} - f_{s1} = \frac{\vec{u}}{\lambda_0}(\overrightarrow{l_{i1}} - \overrightarrow{l_{i2}}) \tag{7}$$

Therefore, the Doppler frequency no longer depends on the direction of scattering. This allows the collection of the scattered wave over a wide angle. To determine the droplet size, the phase difference of the scattered wave at the same scattering angle θ but different elevations is analysed (Fig. 2). If the droplet is perfectly spherical and homogeneous, two locations are enough. However, for real applications a third location is foreseen in order to increase the droplet size measurement range. Finally, the droplet diameter is proportional to the phase difference.

3. Experimental study

The presented simulation model for evaporation was previously verified for single droplets of pure water and saline water using experimental data [2]. To compare the theoretical model of the spray, an experimental test rig was installed.

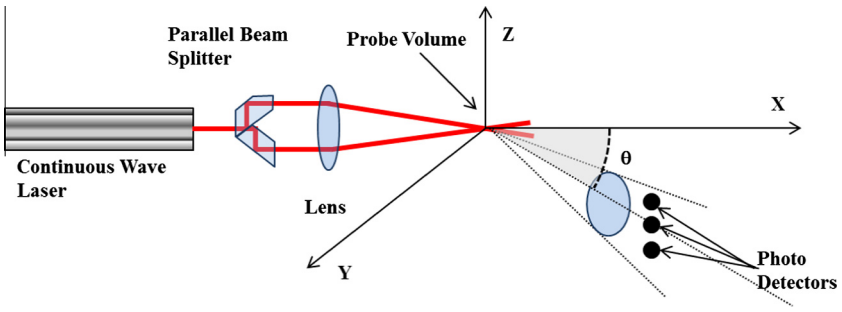

Fig. 2. Dual beam or fringe mode of DPI.

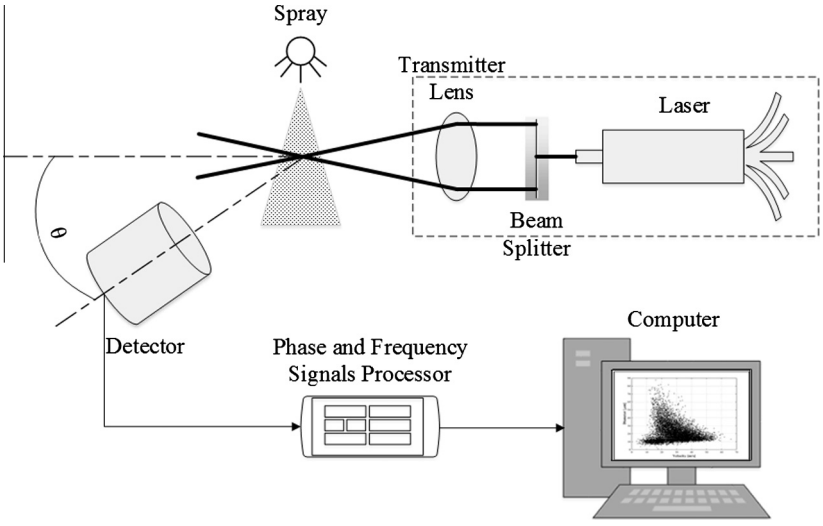

Fig. 3. The test rig installed to monitor the particles in the spray.

3.1. Test rig

The apparatus shown in Fig. 3 was installed in the von Karman Institute for Fluid Dynamics, Belgium. An Artium Technologies Inc. PDI system was used to characterize the particles size and velocity distributions in the spray. The atomizer chosen for the experimental measurements is generally used as a calibrator at the von Karman Institute for several years, and has already been extensively characterized.

In order to select the diameter range and the velocity of the droplets generated by the atomizer, the supplied air pressure should be adjusted. Moreover, the atomizer possesses a specific mechanism allowing varying its outlet orifice diameter. Adjusting the orifice diameter allows a precise regulation of the droplet size. In the PDI settings in this work, the maximum droplet size was chosen as the largest droplet was falling below 80 μm. The main reason is that large droplets have a greater probability to be aspherical, and the droplet asphericity is a source of uncertainty for the PDI measurements. In these conditions the generated spray possesses a solid cone nozzle with the half angle of 40°. Measurements were performed for a water solution with 3% initial NaCl concentration (by mass).

In principle, setting the droplet size and velocity range in the PDI system is not necessary. Nevertheless, in order to increase the accuracy of droplet size measurements a proper choice of the instrument optics (namely the focal length of the emitter and receiver lenses) should be made. Firstly, lenses allowing the measurements of a broad particle size range are chosen, then following the results given by the PDI appropriate lenses are selected to restrict the measurements in the band of interest. In the specific case a couple of lenses allowing measurements between 1 μm and 80 μm has been selected.

As far as the velocity is concerned, the PDI system performs an iterative process in which a set number of signals are used to measure the flow conditions at the beginning of each test. The information about the flow conditions is then used to establish the optimum settings for the signal processor.

To obtain the size distribution of the spray, PDI measurements were performed at different radial positions in the spray (P_1 to P_n) and at two different distances, L from the nozzle as shown in Fig. 4.

Two mercury-in-glass thermometers with the accuracy of 0.5 °C were used to measure the dry and wet-bulb temperatures. The web-bulb temperatures were used to determine the relative humidity.

The total mass flow rate of the nozzle was measured by collecting the sprayed water in a closed container for 5 min. The mass flow rate was then determined by weighting the sprayed water and dividing it by the measuring time. The tests were performed in room condition at 23 °C and 58% relative humidity.

It is important to underline that the PDI measurements have been conducted far enough from the nozzle exit to ensure that the droplet concentration, as well as the droplet sphericity was in the measurable limit of the instrument, meaning that the percentage of accepted measurements was always above 80%.

3.2. Experimental results

In this study several points along the nozzle axis have been measured. It has been noticed that, measurements too close to

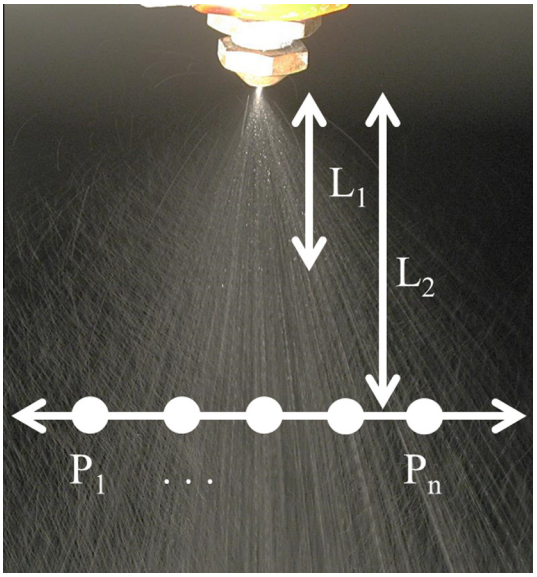

Fig. 4. Test points for the PDI measurements.

the atomizer exit are affected by the presence of liquid ligaments and large droplet density, whilst far away the smallest droplets are entrained by external airflows. As a consequence a trade-off has been made and two distances have been selected: 5 mm and 8 mm from the atomizer exit. It was observed that, as predicted by the theory, the droplet size distribution is not uniform along the spray. This is mainly due to both liquid fragmentation and air entrainment. As an example, the histogram shown in Fig. 5 corresponds to the midpoint of the spray (i.e. its axis) at 5 mm from the nozzle. In order to compare the different test points between each other, the total number of the droplets are normalized by its maximum value.

In Fig. 5, the solid line shows the predicted size histogram whilst the dotted line corresponds to the experimentally obtained results. To simulate the spray by FLUENT, a full cone solid nozzle with the cone half angle of 40° is positioned in a cylindrical fluid domain with a diameter of 0.2 m and length of 0.5 m. The mass flow rate of the spray is 0.298 g/s.

Based on the experimental results the droplet distribution is set to a non-uniform Rosin–Rammler pattern for which [23]:

$$Y = e^{-(d/\bar{d})^n} \tag{8}$$

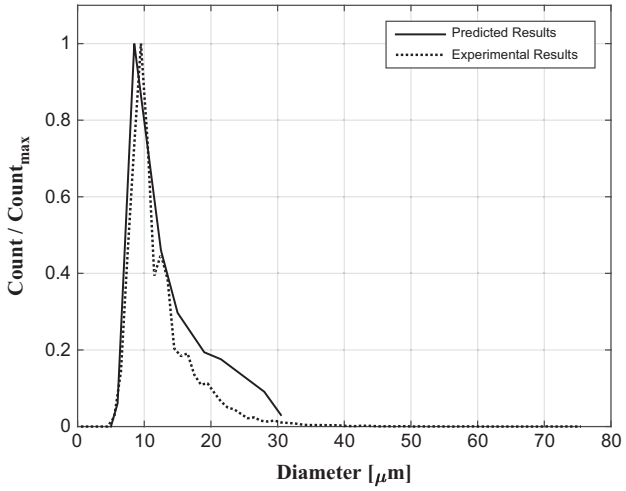

Fig. 5. Diameter histogram at 5 mm from the nozzle.

where Y is the mass fraction of the droplets with greater sizes than d, $\bar{d}$ is the size constant, and n is the size distribution parameter. For the data presented in Fig. 5, the mass fraction of each range of size is shown in Table 1:

In Table 1, the size ranges with number of droplets less than 0.05% of the total amount are neglected. To find the size constant, $\bar{d}$, one can solve Eq. (8) for $\frac{d}{\bar{d}} = 1$, and thus, $Y = e^{-1} \approx 0.368$ [12]. Then, as shown in Fig. 6, using this value for Y gives $\bar{d}$ = 30.85 μm for this spray.

The value of n is determined by solving Eq. (8) $\left(n = \frac{\ln(-\ln Y)}{\ln(d/\bar{d})}\right)$ as 3.38. Using this setup for the ANSYS FLUENT model, the size histogram is accurately predicted at 8 mm from the nozzle, which agrees the experimental results (Fig. 7). Comparing Figs. 5 and 7, it is shown that the sharp tail of the size distribution at 5 mm reaches a more gradual rate at 8 mm.

To compare the sizes measured by PDI with the simulated results, D_{32} (Sauter Mean Diameter (SMD)) is determined for the numerical results obtained from the FLUENT model as follows [24]:

$$D_{32} = \frac{\sum n_i d_i^3}{\sum n_i d_i^2} \tag{9}$$

where n_i is the number of droplets with d_i diameter. To calculate the SMDs of the numerical results, a MATLAB code is developed which computes SMD for concentric rings with 0.5 mm width, at 5 mm and 8 mm from the nozzle (Fig. 8).

The experimental and numerical values of SMD at 5 mm and 8 mm from the nozzle are shown in Figs. 9 and 10, respectively. As shown in these figures, the measurements were performed with 1 mm spacing in the width of the spray, but to increase the resolution of the numerical values, SMDs are determined using 0.25 mm spacing.

The statistical parameters for points P_1 to P_6 in Fig. 9 are shown in Table 2. The maximum diameter and velocity are recorded for P_3 (87.8 μm) and P_4 (73.7 m/s), respectively. More than 16,800 droplets were measured for each point and the minimum percentage of the passed droplets is 74.5% (25.5% rejected).

The measurement shown in Fig. 10 are repeated three times and are the mean values of the three datasets. Using the procedure recommended by Moffat [25], the 95% confidence intervals for the diameter measurements is 4.28% and for the sprayed mass flow rate is 1.59%.

Comparing Figs. 9 and 10 shows that the SMD is transforming from a downward bell-shaped curve to an upward one. A clearer trend is shown by the presented numerical data in Fig. 11. After 5 mm from the nozzle, the sizes at the sides of the spray are predicted slightly larger than the middle ones as the surrounding air entrainment within the spray pushes the smaller droplets towards the centre as the inertia of the small droplets are less than the larger ones. A similar effect was observe by Vetrano et al. [21].

As shown in Fig. 11, going further from the nozzle, the spray width is increasing. As such, the width of the spray is 10.8 mm,

Table 1
Experimental mass fraction of the droplets with greater diameter than d.

Size range (μm)	Count	Droplets mass (μkg)	Mass fraction	Y
0–5.5	0	0.0000	0.000	1.000
5.5–10.5	8003	0.0099	0.059	0.941
10.5–15.5	5961	0.0238	0.142	0.799
15.5–20.5	2474	0.0228	0.136	0.662
20.5–25.5	1276	0.0226	0.135	0.527
25.5–30.5	817	0.0248	0.148	0.378
30.5–35.5	519	0.0248	0.149	0.230
35.5–40.5	336	0.0239	0.143	0.087
40.5–45.5	165	0.0145	0.087	0.000

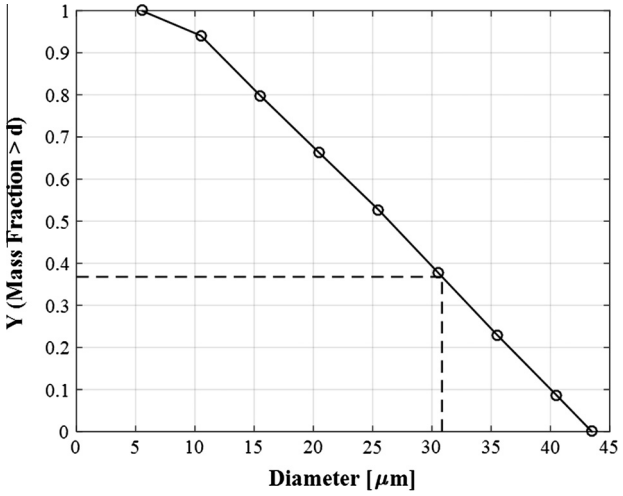

Fig. 6. Determining the size constant, $\bar{d}$.

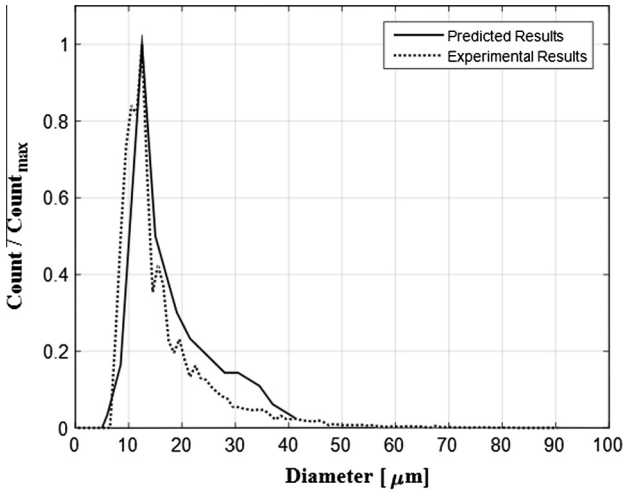

Fig. 7. Diameter histogram at 8 mm from the nozzle.

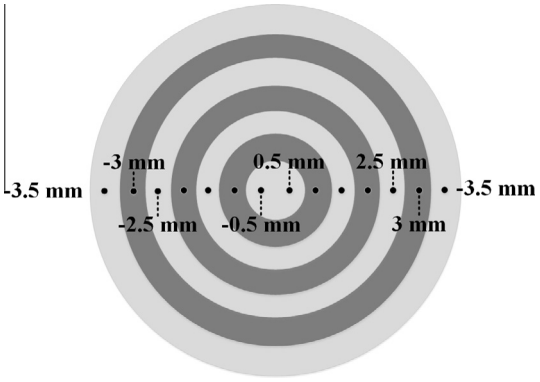

Fig. 8. The 0.5 mm rings to determine SMD at the perpendicular plane 5 mm and 8 mm from the nozzle.

19 mm, and 26.8 mm at 5 mm, 10 mm, and 15 mm from the nozzle, respectively.

Fig. 12 shows the experimental data for mass and diameter of consecutive point at 8 mm from the nozzle. The most populated areas in these plots are triangles in the middle of the scattered part. What stands out in these plots is that the heavier droplets show a lower velocity variation. Also, the droplets with the maximum

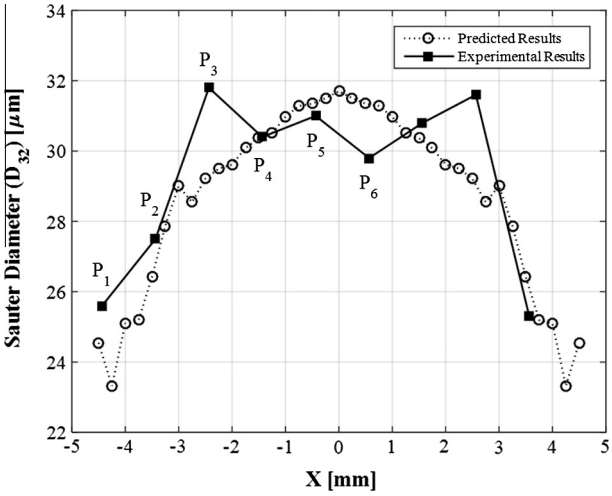

Fig. 9. SMD along the spray at 5 mm from the nozzle.

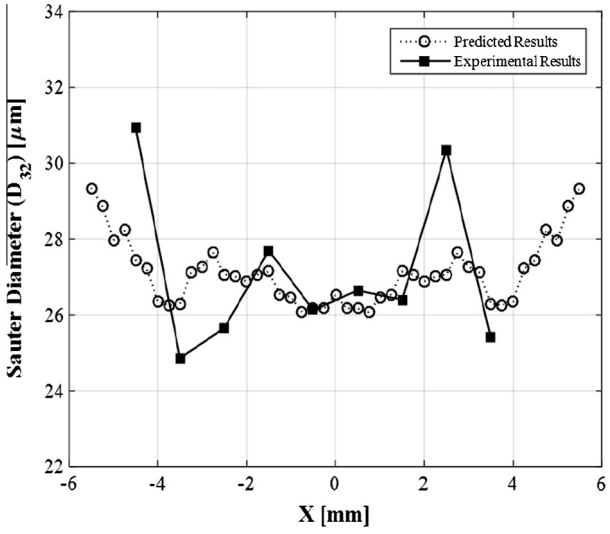

Fig. 10. SMD along the spray at 8 mm from the nozzle.

Table 2
Statistical diameters and velocities of the six tested points 5 mm from the nozzle.

	P_1	P_2	P_3	P_4	P_5	P_6
D_{10} (μm)	17.4	17.4	20.6	20.4	21	16.2
D_{20} (μm)	19.1	19.4	23	22.4	23.1	18.8
D_{30} (μm)	21	21.8	25.6	24.8	25.5	21.9
D_{32} (μm)	25.6	27.5	31.8	30.4	31	29.8
Diameter min (μm)	7.4	7.5	7.6	7.8	8.2	7.3
Diameter max (μm)	74	84	87.8	83.9	82.9	82.4
Average velocity (m/s)	21.6	30.0	35.4	36.1	28.7	18.8
Velocity min (m/s)	0.3	0.6	2.2	7.4	2.7	0.2
Velocity max (m/s)	51.1	67.6	72.0	73.7	67.3	48.3
Total counts	17,721	18,884	17,154	17,036	16,866	20,117
Passed droplets (%)	82.9	74.5	74.9	77.7	78.37	75.7

Reynolds numbers are located on the right side of the triangle. In other words, both the highest and lowest velocities correspond to the lighter droplets because the heavier the droplet, the higher the inertia and thus the higher the strength to the flow field.

4. Numerical simulation

A practical natural draft dry cooling tower consists of a tower containing heat exchangers, which are cooled by the inflowing

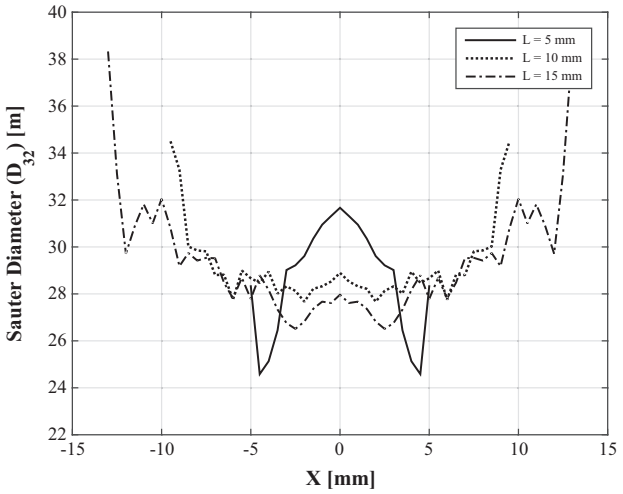

Fig. 11. Upward bell-shaped trend of the SMD after 5 mm from the nozzle (numerical data).

ambient air. To improve the performance, water sprays are used to decrease the inlet air temperature. In a vertical cooling tower, the water is sprayed in an upward airflow, which then approaches the heat exchangers [26]. To simulate a spray assisted natural draft dry cooling tower a simplified geometry with a single nozzle in a 5 m diameter vertical cylinder of 8 m length is considered. As shown in Fig. 13, one end of the domain (cylinder) reaches the heat exchanger surface.

Since there are multiple nozzles working in a spray assisted dry cooling tower, nozzle distribution and nozzle-to-nozzle interaction are two important parameters. Smrekar et al. showed that by improving the spray arrangement design an optimal water distribution with a constant water/air mass flow rate can be achieved which can improve the efficiency by 5.5% [27]. However as the current study focuses on a like-for-like comparison of performances of spray cooling system at different initial and ambient conditions, the canonical geometry from Fig. 13, representative of the flow pattern in an ideal cooling tower with negligible nozzle to nozzle interaction is used. This allows the performance change to be evaluated in isolation.

In Fig. 13, the shown full cone nozzle injects in the positive Z direction. The model includes gravity acting in the negative Z direction. Inlet air properties correspond to a hot summer day in Miles, Queensland, 40 °C and 44% relative humidity [28]. The saline water droplets with 3% initial NaCl concentration (by mass) are introduced to the CFD simulation using the method explained in [2]. To be able to perform a comparison between the different simulated cases, the initial droplet distribution is kept uniform. The nozzle is a solid full cone type with a half angle of 40°. According to the geometry of cooling towers and ambient conditions, different designers may apply different types of nozzles.

A smooth structured mesh of 281,280 elements is used. Using the grid convergence index (GCI) method explained by Roache [29] a spatial convergence examination is performed on the numerical grid. The GCI is defined as [30]:

$$\mathrm{GCI} = \frac{F_s|\varepsilon|}{r^p - 1} \tag{10}$$

where F_s is a safety factor which is recommended to be 3.0 for two grids comparison [30]. ε is the relative error of the solutions, r is the grid refinement ratio ($r > 1$), and p is the order of convergence which is set to two. The grid refinement ratio was set to 1.33. To determine the GCI, the region of the domain immediately downstream of the nozzle is used, because least stability was observed in this region due to droplet generation. Therefore, a 0.5 m diameter cylinder with a length of 1 m was considered. The GCI for important variable in regard with the nature of the current problem are listed in Table 3, which shows that the finer mesh size or decreasing the element number has negligible influence on the results.

Fig. 14 shows the contours of temperature and relative humidity at an upward air velocity of 1.5 m/s. The spray mass flow rate is 0.02 kg/s and the droplets are generated with an initial diameter of

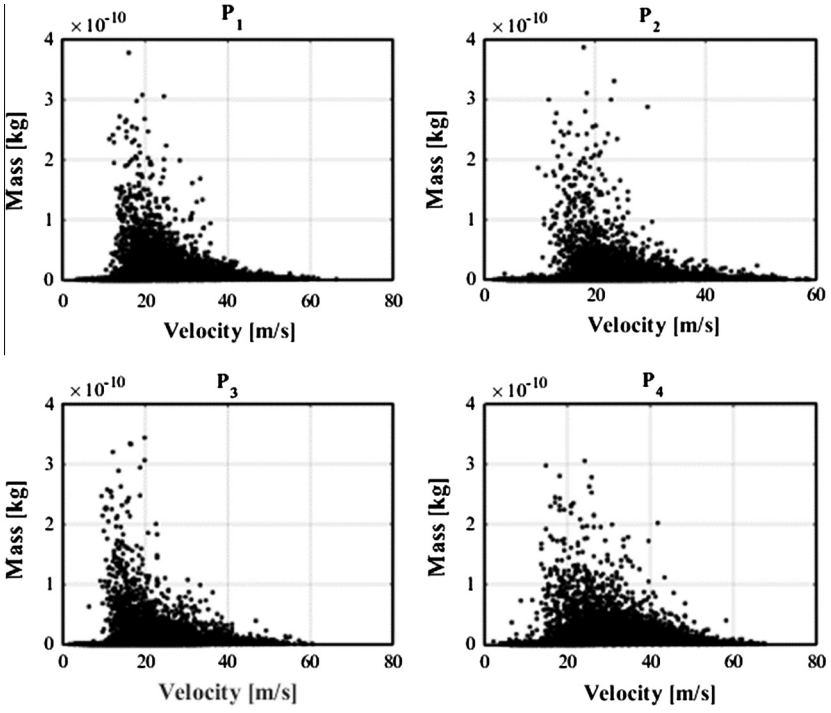

Fig. 12. Particle tracking; experimental data for mass versus velocity of each droplet for the four tested points 8 mm from the nozzle.

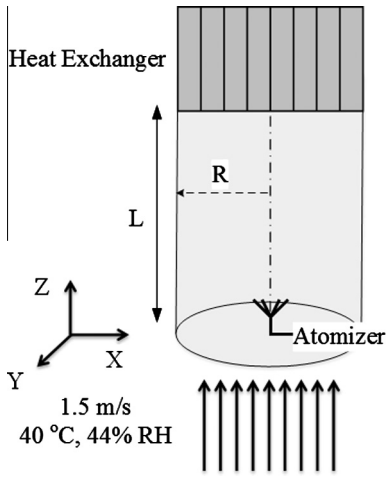

Fig. 13. Geometry of the simulated system.

50 μm. The minimum temperature and maximum relative humidity achieved by the single nozzle are 26.5 °C and 89.4%, respectively around 1.8 m from the nozzle. Further away from the nozzle, there is a more uniform temperature and relative humidity. With increasing distance, wider area is affected by the spray.

The more uniform temperature profiles further from the nozzle are shown in Fig. 15. Relative to the incoming air at 40 °C, there is a dramatic decrease (13.5 °C) at the middle of the stream 2 m from the nozzle. Radial variation of temperature declines at 4 m and 6 m and consequently reaches to 4.8 °C at 8 m from the nozzle. At the same time the area affected by the cooling increases.

5. Sensitivity investigation

After performing the experimental study on a real-life saline water spray, the CFD model was improved. For example, setting the practical specification for the nozzle resulted in more reliable outputs from the simulation. After strengthening the CFD model, an analysis on the results was made.

According to the four stages model presented by Sadafi et al. [10] for the evaporation of a single solid containing droplet, the presence of the solid crust on droplets surfaces is the beginning of the drying (fourth) stage. In this stage of evaporation a solid layer covers the droplet whilst the inner wet-core is still evaporating (shrinking). This solid crust acts as an insulator, which reduces the total heat transfer rate. Also, it reduces the risk of deposition of a wet solution droplet on the heat exchanger and corrosion of the metal surfaces due to its dry surface. Therefore, the location which the crust forms around the droplet, is an important variable for the spray. After this location, there is a dry stream of solid particles, whilst there is a wet flow before this location. To determine this length from the nozzle (L_{wet}, wet length) the model monitors the travelling droplets.

In addition to wet length, cooling performance of the spray is another important parameter. It is defined as:

$$\eta_{Cooling} = \frac{T_{in} - T_{out}}{T_{in} - T_{wb}} \tag{11}$$

Table 3
Grid convergence index (GCI) for important variables.

Variable (at 1 m)	GCI (%)
Temperature of centre point	0.566
Gas velocity in the midpoint	2.083
Velocity of droplet "1"	2.075
Mean gas temperature	0.155
Mass fraction of H_2O	0.012

where T_{in} and T_{wb} are initial temperature of the gas and wet bulb temperature of environment, respectively. T_{out} is the outlet temperature of the air, which is cooled by the spray. To have an appropriate gauge for outlet temperature, the area weighted mean temperature in a virtual disk of 2 m diameter and 6 m from the nozzle is considered.

To investigate the influence of different spray parameters and ambient conditions on the wet length and cooling efficiency, 13 cases were defined and simulated in addition to the main case (case 1) as shown in Table 4. In each case, one spray parameter is perturbed by 10%, relative to case 1.

Here, the influence of each perturbation on the wet length and cooling efficiency is analysed.

5.1. Wet length

Fig. 16 shows the influences of the ambient and droplet initial conditions on the wet length. Case 1, is used as the reference case with a wet length of 4.68 m. The bars show the effect of increasing and decreasing the parameters.

The changing parameters are divided into two groups. The first group includes: gas temperature, relative humidity, and air velocity (ambient parameters). A designer may have no control on these parameters. However, the influence of these parameters on the wet length should be investigated. Here, 10% dryer air stream achieved a shorter wet length (4.37 m) compared to case 3, with 10% hotter gas temperature (4.45 m). However, case 2 with cooler gas temperature and case 5 with higher relative humidity give a similar wet length (approximately 5.1 m). Among the three parameters of this group, air velocity shows a more consistent effect for both 10% increase and decrease.

The second group of parameters is droplets initial diameter, mass flow rate of sprayed water, and the initial concentration of salt. These are the design parameters which may be adjusted to achieve a better design. Droplets initial diameter influences the wet length the most. Due to d^2 law, the evaporation and thus the wet length is proportional to diameter squared [11]. Therefore, the wet length is strongly affected by the initial droplet diameter. As such, the cases with 5 μm larger and smaller diameters correspond to 5.25 m and 4.3 m wet lengths, respectively. A 10% change in the mass flow rate of sprayed water has a weaker influence on the wet length compared to the diameter. Whereas 10% reduce in mass flow rate, results in only 0.15 m reduce in the wet length. Among the three design parameters, the initial concentration of the salt has the lowest impact. According to Fig. 16, doubling initial concentration reduces the wet length by only 0.15 m.

To find a general correlation between the wet length and the initial and ambient conditions, the non-dimensional numbers involved in the problem are found using Buckingham Π theorem. Considering the wet length, the non-dimensional groups are: a temperature ratio $\Omega = \frac{T_{0,d}}{(T_g - T_{wb})}$ that includes the effect of relative humidity by involving T_{wb}, water–air mass flow rate ratio, a flux ratio $\Psi = \frac{k_g (T_g - T_{wb})}{Du^3 \rho_g}$, Reynolds Number, Prandtl number, and initial concentration of salt.

Numerical data collected as part of the current study shows that a polynomial relationship exists between dimensionless wet length and the dimensionless variables. The polynomial response surface approximation method [31] was used to find a correlation. A *t*-test was also used to eliminate the insignificant terms (less than 5% of significance) from the polynomial. The resulting correlations is:

$$\frac{L_{wet}}{D_{d,0}} = 1345.5\Omega - 1.7 \times 10^4 \left(\frac{\dot{m}_w}{\dot{m}_g}\right)^{-0.14} - 9.8 \times 10^4 \times \Psi^{0.13} + 3.6 \times 10^5 \tag{12}$$

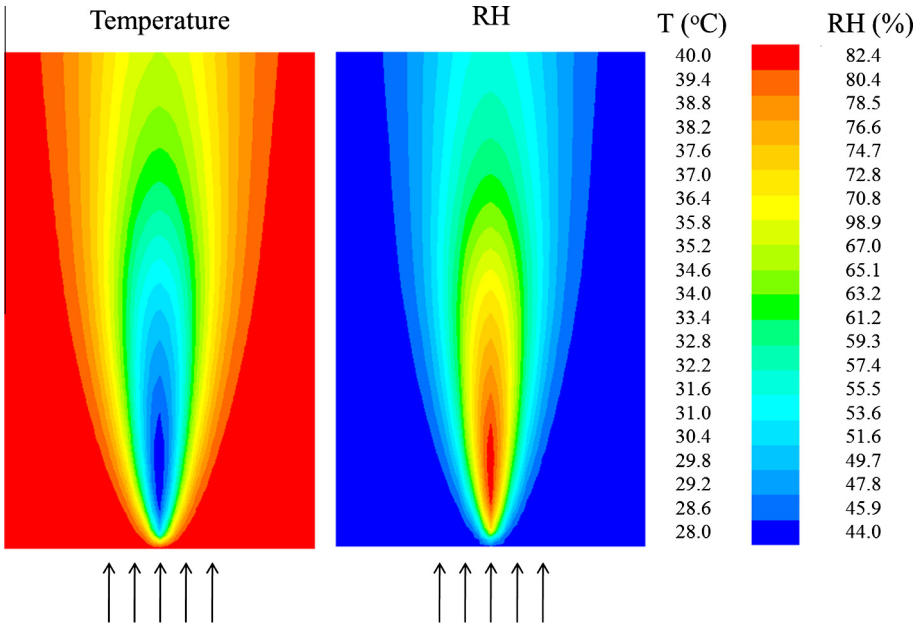

Fig. 14. Contours of temperature and relative humidity for the simulated condition (40 °C, 44% relative humidity, 1.5 m/s air velocity).

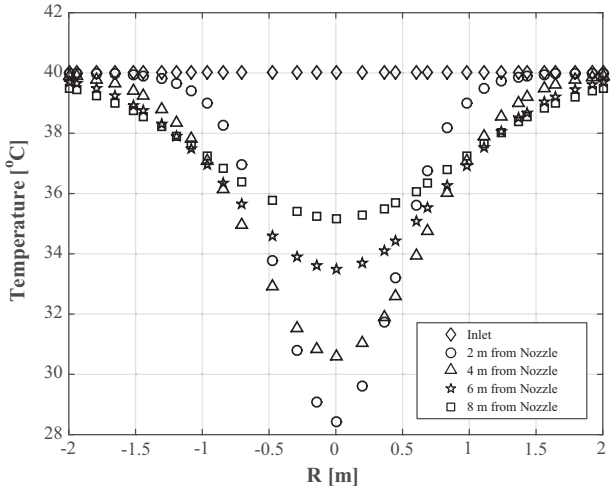

Fig. 15. Temperature variation in the spray width at different section.

Based on hypothesis testing, this final correlation is a good match to the numerical training data. The *p*-value corresponding to the simulated data and the values obtained from Eq. (12) is 0.71. Fig. 17 shows the results obtained from the simulation as well as the data predicted in accordance to Eq. (12).

Fig. 17 demonstrates that Eq. (12) is a reliable prediction of L_{wet} for saline water spraying. This correlation is a useful tool to design a spray cooling systems, as it allows the length of the wet spray region to be predicted.

5.2. Cooling efficiency

Fig. 18 shows the influence of different initial and ambient conditions on the cooling efficiency. Case 1 is considered as the reference case with 33.9% cooling efficiency.

According to Fig. 18, a 10% reduction in inlet air temperature (as shown in Fig. 1) to 36 °C, improves cooling efficiency by 2.4%. Here, relative humidity shows a stronger influence on the cooling efficiency. A 10% increase in relative humidity, leads to 3.6% raise in cooling efficiency. This is due to a change in wet bulb temperature. According to Eq. (11), at a constant dry bulb temperature, an increase in wet bulb temperature (relative humidity) results in an increase in the cooling efficiency. Similarly to the wet length, among the three ambient parameters, air velocity has the weakest influence on the cooling efficiency (less than 2%).

Among the design parameters, the cooling efficiency shows a weak sensitivity to the initial diameter. This is because all the cases with the initial diameters of 45 μm, 50 μm, and 55 μm have the identical mass flow rate of 0.02 kg/s and almost the same evapo-

Table 4
Initial conditions of the simulated cases.

Case number	Ambient temperature (°C)	RH (%)	Air velocity (m/s)	Initial droplet size (μm)	Mass flow rate (kg/s)	Initial concentration (%)
Case 1	40	44	1.5	50	0.02	3
Case 2	36	44	1.5	50	0.02	3
Case 3	44	44	1.5	50	0.02	3
Case 4	40	39.6	1.5	50	0.02	3
Case 5	40	48.4	1.5	50	0.02	3
Case 6	40	44	1.35	50	0.02	3
Case 7	40	44	1.65	50	0.02	3
Case 8	40	44	1.5	45	0.02	3
Case 9	40	44	1.5	55	0.02	3
Case 10	40	44	1.5	50	0.018	3
Case 11	40	44	1.5	50	0.022	3
Case 12	40	44	1.5	50	0.02	1
Case 13	40	44	1.5	50	0.02	5
Case 14	40	44	1.5	50	0.02	6

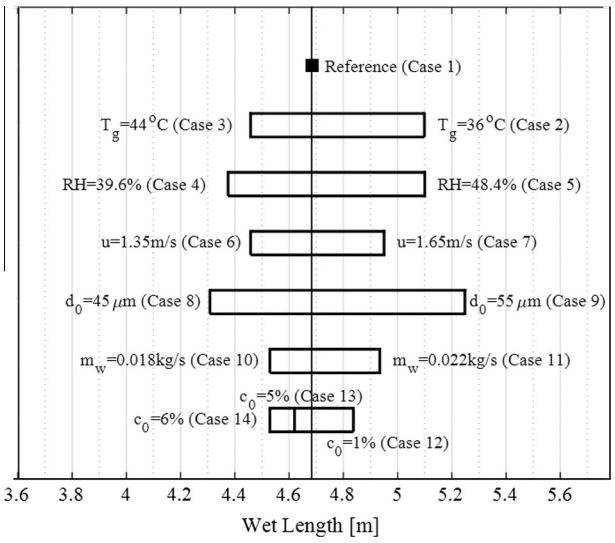

Fig. 16. Influence of initial and ambient conditions on the wet length.

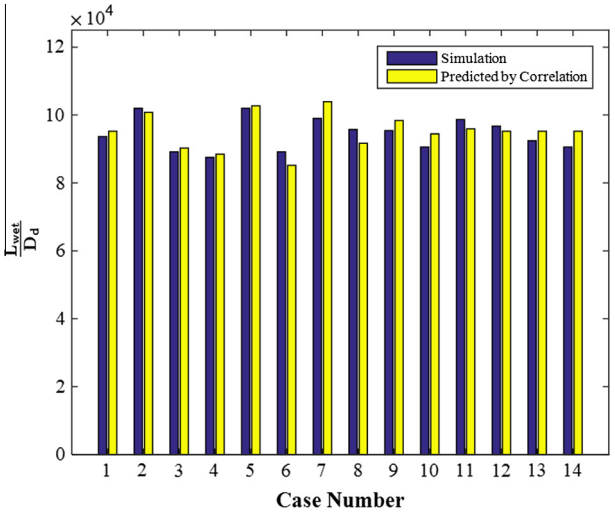

Fig. 17. Presented correlation to determine the wet length.

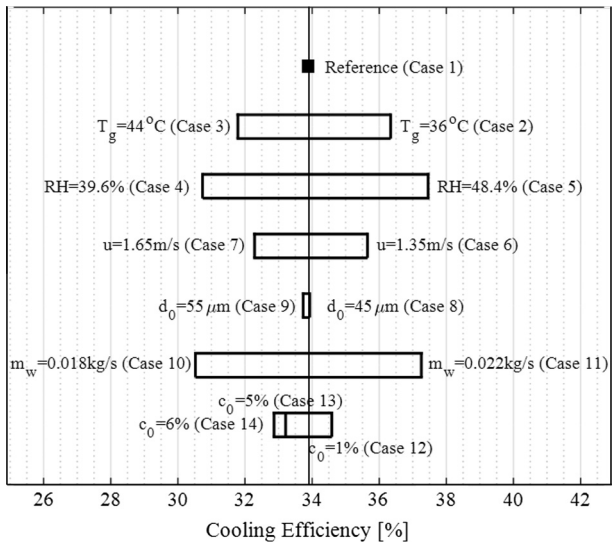

Fig. 18. Influence of initial and ambient conditions on the cooling efficiency.

rated water mass at the considered plane for cooling efficiency calculation. In contrast, sprayed water mass flow rate influences the cooling efficiency the most. A 10% increase in water mass flow rate, achieves 3.4% higher cooling efficiency. Fig. 18 shows that the cooling efficiency is a function of saline water initial concentration as well. Here, the cases using 1%, 3%, 5%, and 6% initial concentration by mass correspond to 34.58%, 33.90%, 33.21%, and 32.86% cooling efficiencies as the net mass of water is decreasing. Therefore, the heat transferred from the gas to water in the spray decreases proportionally and thus the cooling efficiency drops.

Performing the dimensionless analysis on the cooling efficiency gives the followings non-dimensional groups: Reynolds number, *Re*, water-air mass flow rate ratio, the flux ratio Ψ, and initial concentration of salt.

Here, the simulated results for cooling efficiency are a polynomial function of the involved non-dimensional variables. Using polynomial response surface approximation method [31], and eliminating the non-significant terms, the following correlation was obtained:

$$\eta_{Cooling} = 337.1Re^{-0.1} + 1.89\times10^{5}\left(\frac{\dot{m}_w}{\dot{m}_g}\right)^{1.48} - 136.8\Psi^{0.085} - 17.1(1-c_0)^{0.79} - 31.4 \quad (13)$$

Fig. 19 shows the predicted data in accordance to Eq. (13) as well as the simulated results. The *p*-value corresponding to the simulated data and the values obtained from Eq. (13) is 0.49. The correlation in Eq. (13) is a practical tool for designers to improve the cooling efficiency.

Compared to the power of the other terms, the mass fraction ratio has the largest power which shows that the cooling efficiency is more sensitive to water mass flow rate as the most effective design parameter.

6. Discussion

After validating the presented numerical model against the experimental study in this work, the two correlations accurately predict the wet length and cooling efficiency. Analysis on the two correlations show that although a decrease in droplets size

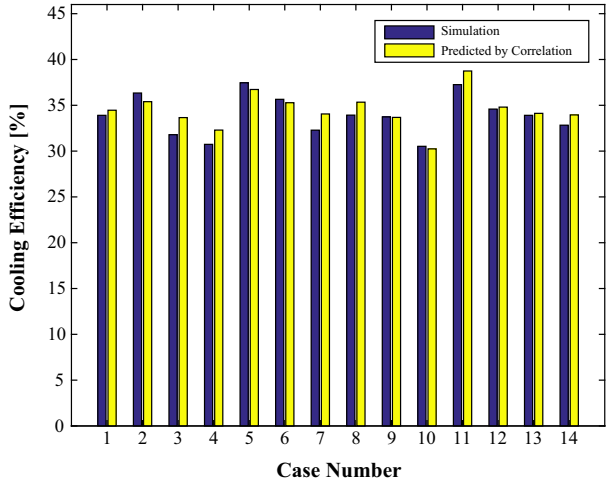

Fig. 19. Presented correlation to determine the cooling efficiency.

and water mass flow rate decreases the wet length, at the same time it also deteriorates the cooling efficiency. Therefore, a more convenient tool is required to take both wet length and cooling efficiency into consideration at the same time.

Fig. 20 shows the combined trends of wet length to diameter ratio and cooling efficiency as the design parameters (droplet initial diameter, mass flow rate of water, initial salt concentration) are varied. The data in Fig. 20 corresponds to constant ambient conditions (T_g = 40 °C, RH = 40%, u_g = 1.5 m/s). However, the design parameters including droplet diameter, water mass flow rate of spray, and initial concentration of salt are changing. Therefore, the data for cases 2–7 in Table 4 are excluded, but to obtain a higher validity, 8 new cases are added to Fig. 20 at the same ambient conditions.

The shown curves are obtained using the presented correlations in Eqs. (12) and (13). The solid curves correspond to the constant water mass flow rate of spray, and the dotted curves are related to constant diameter of the droplets. Moving from a low mass flow rate to a high one on a constant diameter curve, achieves an improved cooling efficiency, but a longer wet length. Also, travelling on a constant mass flow rate curve and decreasing the diameter, leads to an increase in cooling efficiency and decrease in wet length. Since generating smaller droplets are limited to the available nozzles in the market, a designer should find an efficient design preferably on the top left corner of Fig. 20, because taking the wet length and the cooling efficiency into consideration, the best designs locate at this region.

Fig. 20 allows a designer to evaluate the design limitations and choose the best design. For example, in a compact design where the designer faces short distance between the nozzle and the heat exchangers, the case with the short wet length of 4.2 m and 30.8% cooling efficiency may be favourable. Here, the design suffers from a lower cooling efficiency to receive a shorter wet length which avoids the contact of wet droplets and heat exchangers.

In a cooling tower with a large enough distance between the nozzles and heat exchangers, a high water mass flow rate condition would be favourable to achieve the highest cooling efficiency of 37.3% at the expense of a long wet length of 4.9 m. In other words, increasing the saline water volume used for spray cooling achieves the desirable result whilst it is not only free of charge, but also leads to pure water preservation.

Therefore, according to the a certain circumstances a designer may choose a design point with a low cooling efficiency and low but short wet length, or an improved efficiency but long wet length. In many cases an optimum performance may be chosen to achieve the best design.

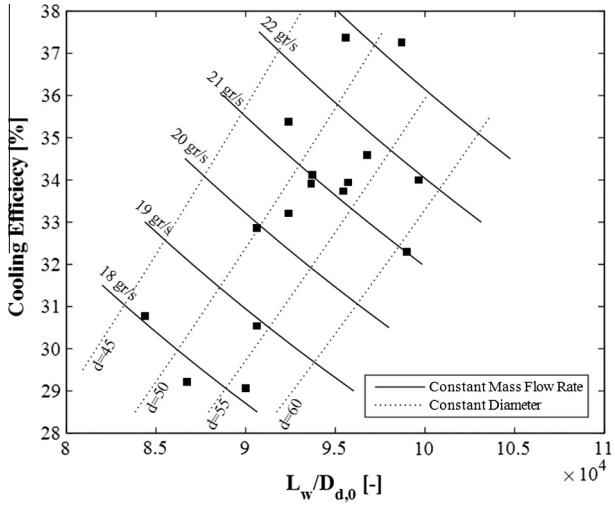

Fig. 20. Constant mass flow rate and concentration curves. Data obtained from evaluating correlations in Eqs. (12) and (13) at a the following ambient conditions (T_g = 40 °C, RH = 40%, u_g = 1.5 m/s).

7. Conclusion

A PDI study was performed and the experimental results were compared to numerical data obtained from the presented CFD simulation. This proved the suitability of the model to investigate the performance of saline spray in cooling towers.

Next, a single solid full cone spray was simulated in a geometry representative of cooling tower flow. Results from a sensitivity study investigating the effects of ambient conditions and spray specification on cooling performance, showed that initial size of droplets and water mass flow rate have the largest impact on the minimum distance between nozzle and heat exchangers (wet length) and cooling efficiency, respectively. The wet length ranged between 4.3 m and 5.25 m. Finally by performing a non-dimensional analysis two dimensionless correlations for wet length and cooling efficiency were created. These gave a new insight into trends relating to saline water spray cooling systems. Looking at the overall trends, it was observed that increasing the saline water mass flow rate yields the best compromise. Using saline water instead of fresh water results in performance improvement and budget saving due to saving in natural water cost and generating excess electricity.

Acknowledgements

This research was performed as part of the Australian Solar Thermal Research Initiative (ASTRI), a project supported by the Australian Government, through the Australian Renewable Energy Agency (ARENA) and was funded by the Queensland Geothermal Energy Centre of Excellence (QGECE) Travel Fellowship. The warm hospitality of the von Karman Institute for Fluid Dynamics in Belgium, during this travel fellowship is highly appreciated.

Appendix A. Supplementary material

Supplementary data associated with this article can be found, in the online version, at http://dx.doi.org/10.1016/j.enconman.2015.11.025.

References

[1] Dolan MD, Roberts DG. Hybrid solar-fossil systems for large-scale solar energy storage. In: First australian workshop on solar thermal chemical and industrial processes. Adelaide, Australia; 2013.
[2] Sadafi MH, Jahn I, Hooman K. Cooling performance of solid containing water for spray assisted dry cooling towers. Energy Convers Manage 2015;91:158–67.
[3] Ashwood A, Bharathan D. Hybrid cooling systems for low-temperature geothermal power production. Golden, CO: National Renewable Energy Laboratory; 2011. p. 1–62.
[4] Nápoles-Rivera F et al. Simultaneous optimization of energy management, biocide dosing and maintenance scheduling of thermally integrated facilities. Energy Convers Manage 2013;68:177–92.
[5] Ohwaki T, et al. Aluminum alloy material having an excellent sea water corrosion resistance and plate heat exchanger. Google Patents; 2014.
[6] Kronenberg G, Lokiec F. Low-temperature distillation processes in single- and dual-purpose plants. Desalination 2001;136(1–3):189–97.
[7] Rubio D, Casanueva JF, Nebot E. Assessment of the antifouling effect of five different treatment strategies on a seawater cooling system. Appl Therm Eng 2015;85:124–34.
[8] Rao R, Patel V. Optimization of mechanical draft counter flow wet-cooling tower using artificial bee colony algorithm. Energy Convers Manage 2011;52(7):2611–22.
[9] Liu L, Li Y, Wang F. Corrosion behavior of metals or alloys with a solid NaCl deposit in wet oxygen at medium temperature. Sci China Technol Sci 2012;55(2):369–76.
[10] Sadafi MH et al. Theoretical and experimental studies on a solid containing water droplet. Int J Heat Mass Transf 2014;78(1):25–33.

[11] Sadafi MH et al. A theoretical model with experimental verification for heat and mass transfer of saline water droplets. Int J Heat Mass Transf 2015;81:1–9.
[12] ANSYS FLUENT® Academic Research, Release 14.0; 2011.
[13] Vetrano M-R, et al. Correlation law for SMD in high viscous liquids. In: 22nd European conference on liquid atomization and spray systems ILASS08; 2008.
[14] Foissac A et al. Experimental measurements of droplet size and velocity distributions at the outlet of a pressurized water reactor containment swirling spray nozzle. Experimental validation and application of CFD and CFMD codes to nuclear reactor safety issues (XCFD4NRS-3). Washington DC; 2010. p. 14–6.
[15] Xie JL et al. Thermal effects on a pressure swirl nozzle in spray cooling. Int J Heat Mass Transf 2014;73:130–40.
[16] Pawar S et al. Numerical and experimental investigation of induced flow and droplet–droplet interactions in a liquid spray. Chem Eng Sci 2015;138:17–30.
[17] Nijdam JJ et al. Lagrangian and Eulerian models for simulating turbulent dispersion and coalescence of droplets within a spray. Appl Math Model 2006;30(11):1196–211.
[18] ANSYS FLUENT theory guide; 2011.
[19] Morsi S, Alexander A. An investigation of particle trajectories in two-phase flow systems. J Fluid Mech 1972;55(02):193–208.
[20] Sadafi MH et al. On the influence of low-power laser source on the evaporation of single droplets: experimental and numerical approaches. In: 7th international exergy, energy and environment symposium. Valencinnes, France; 2015.
[21] Vetrano M et al. Characterization of a non-isothermal water spray by global rainbow thermometry. Exp Fluids 2006;40(1):15–22.
[22] Anthoine J et al. Measurement techniques in fluid dynamics: an introduction. 3rd ed. Rhode Saint Genèse: von Karman Institute for Fluid Dynamics; 2009.
[23] Vesilind PA. The Rosin-Rammler particle size distribution. Resour Recovery Conserv 1980;5(3):275–7.
[24] Merkus HG. Particle size measurements: fundamentals, practice, quality, vol. 17. Springer Science & Business Media; 2009.
[25] Moffat RJ. Describing the uncertainties in experimental results. Exp Thermal Fluid Sci 1988;1(1):3–17.
[26] Kröger DG. Air-cooled heat exchangers and cooling towers. Tulsa, Okl: Pennwell Corp; 2004.
[27] Smrekar J, Oman J, Širok B. Improving the efficiency of natural draft cooling towers. Energy Convers Manage 2006;47(9):1086–100.
[28] http://www.bom.gov.au/; 2014 [29-08-2014].
[29] Roache PJ. Fundamentals of computational fluid dynamics. Albuquerque, NM: Hermosa Publishers; 1998. 1998.
[30] Slater JW. Examining spatial (grid) convergence. Public tutorial on CFD verification and validation, vol. 86. MS: NASA Glenn Research Centre; 2006.
[31] Donovan JL. A.F.I.O.T.W.-P.A.O.S.O. ENGINEERING. An application of response surface methodology to a macroeconomic model. Defense Technical Information Center; 1985.